Theoretical Investigation of H$_2$ Combustion on αAl$_2$O$_3$ Support

by Jennifer Synowczynski, Jan W. Andzelm, and D. G. Vlachos

NOTICES

Disclaimers

The findings in this report are not to be construed as an official Department of the Army position unless so designated by other authorized documents.

Citation of manufacturer's or trade names does not constitute an official endorsement or approval of the use thereof.

Destroy this report when it is no longer needed. Do not return it to the originator.

Army Research Laboratory

Aberdeen Proving Ground, MD 21005

Theoretical Investigation of H$_2$ Combustion on αAl$_2$O$_3$ Support

Jennifer Synowczynski and Jan W. Andzelm
Weapons and Materials Research Directorate, ARL

D. G. Vlachos
University of Delaware

REPORT DOCUMENTATION PAGE		*Form Approved* *OMB No. 0704-0188*

Public reporting burden for this collection of information is estimated to average 1 hour per response, including the time for reviewing instructions, searching existing data sources, gathering and maintaining the data needed, and completing and reviewing the collection information. Send comments regarding this burden estimate or any other aspect of this collection of information, including suggestions for reducing the burden, to Department of Defense, Washington Headquarters Services, Directorate for Information Operations and Reports (0704-0188), 1215 Jefferson Davis Highway, Suite 1204, Arlington, VA 22202-4302. Respondents should be aware that notwithstanding any other provision of law, no person shall be subject to any penalty for failing to comply with a collection of information if it does not display a currently valid OMB control number.
PLEASE DO NOT RETURN YOUR FORM TO THE ABOVE ADDRESS.

1. REPORT DATE *(DD-MM-YYYY)*	2. REPORT TYPE	3. DATES COVERED *(From – To)*
November 2008	Summary	

4. TITLE AND SUBTITLE	5a. CONTRACT NUMBER
Theoretical Investigation of H_2 Combustion on αAl_2O_3 Support	
	5b. GRANT NUMBER
	5c. PROGRAM ELEMENT NUMBER

6. AUTHOR(S)	5d. PROJECT NUMBER
Jennifier Synowczynski, Jan W. Andzelm (ARL), and D. G. Vlachos (University of Delaware)	
	5e. TASK NUMBER
	5f. WORK UNIT NUMBER

7. PERFORMING ORGANIZATION NAME(S) AND ADDRESS(ES)	8. PERFORMING ORGANIZATION REPORT NUMBER
U.S. Army Research Laboratory ATTN: AMSRD-ARL-WM-MA Aberdeen Proving Ground, MD 21005	ARL-TR-4642

9. SPONSORING/MONITORING AGENCY NAME(S) AND ADDRESS(ES)	10. SPONSOR/MONITOR'S ACRONYM(S)
	11. SPONSOR/MONITOR'S REPORT NUMBER(S)

12. DISTRIBUTION/AVAILABILITY STATEMENT
Approved for public release; distribution unlimited.

13. SUPPLEMENTARY NOTES

14. ABSTRACT

Based on Density Functional Theory – Generalized Gradient Approximation (DFT-GGA) calculations, we provide a theoretical model for the effect of the catalytic support (alpha alumina oxide (αAl_2O_3)) on the dissociation of molecular hydrogen (H_2), molecular oxygen (O_2), hydroxyl (OH), water (H_2O), and the surface diffusion of oxygen and hydrogen species along the αAl_2O_3 (0001) surface. These processes are key to understanding the "inverse spillover effect" that occurs during hydrogen combustion on alumina surfaces. Our results indicate the dissociation of O_2 is not thermodynamically favored on the αAl_2O_3 surface. However, both H_2 and H_2O can dissociate, forming hydroxyls with oxygen atoms in the second atomic layer. Once dissociated, oxygen species can diffuse locally but encounter a large barrier to long-range surface diffusion in the absence of defects or other species. In contrast, the barrier to the long-range surface diffusion of hydrogen is modest under ideal conditions.

15. SUBJECT TERMS
Inverse spillover effect, Al_2O_3, H_2 combustion, O, OH, H_2O adsorption

16. SECURITY CLASSIFICATION OF:			17. LIMITATION OF ABSTRACT	18. NUMBER OF PAGES	19a. NAME OF RESPONSIBLE PERSON
			UU	22	Jennifier Synowczynski
a. REPORT	b. ABSTRACT	c. THIS PAGE			19b. TELEPHONE NUMBER *(Include area code)*
U	U	U			(410) 306-0750

Standard Form 298 (Rev. 8/98)
Prescribed by ANSI Std. Z39.18

Contents

List of Figures

List of Tables

Acknowledgments

INTENTIONALLY LEFT BLANK.

1. Introduction

As the electronics behind the future warrior systems become more sophisticated, the weight of the batteries is an ever-increasing burden. One solution is to create a compact micro-burner device as shown in figure 1 (Norton et al., 2004) that combusts a higher energy density fuel such as methane (energy density = 3053 W-hr/kg compared to 125 W-hr/kg for lithium (Li)-ion batteries) and converts the released enthalpy into electrical power.
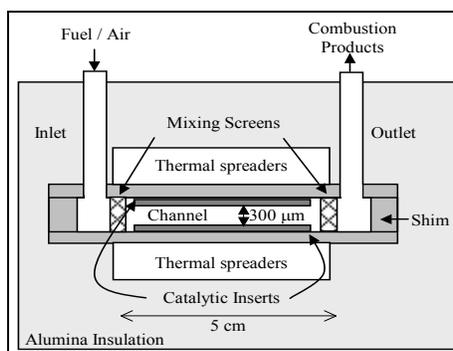
Figure 1. Micro-burner schematic.

Note: The catalytic insert consists of nanosized platinum (Pt) dispersed within porous alumina (Al_2O_3).

Although there are many computational studies that detail the complete hydrogen (H_2) combustion mechanism for reactant and product species interacting with the catalytically active Pt cluster (Mhadeshware and Vlachos, 2007), few studies consider the effect of the Al_2O_3 support. New reaction pathways can arise due to support surface termination and reactivity at the Al_2O_3/Pt interface. One example of such a pathway is the "inverse spillover effect" (ISE), which occurs when water (H_2O) chemisorbs or dissociates on the support forming mobile species that can migrate to the catalytically active particle and further promote combustion. Experimental evidence for ISE comes from the work of Wang et al. (1996) who demonstrated that carbon monoxide (CO) can liberate H_2 from an H_2O bound to Al_2O_3 support. In this report, we seek to augment the current model for H_2 micro-combustion to include reactions that are initiated on the catalytic support. Specifically, we propose a mechanism by which H_2O and H_2 dissociate on the support forming hydroxyl groups, which can further dissociate and diffuse to the catalytic particle.

2.   Model Parameters and Validation

2.1   Alpha-alumina oxide (αAl$_2$O$_3$) Surface Termination

Our model (figure 2) consisted of a nine atomic layer thick, aluminum (Al)-terminated (0001) slab that is repeated under periodic boundary conditions as a 2x2 supercell with P1 symmetry and a 30Å vacuum layer to prevent any interaction between periodic images. We chose this surface based on the availability of experimental and theoretical data in the literature as well as the work of Marmier et al. (2004), who calculated surface phase diagrams as a function of temperature and the oxygen (O$_2$) and H$_2$ partial pressures for several different crystal orientations and surface terminations. The lattice parameters for the rhombohedral unit cell (a=b= 4.749 Å, c=12.991 Å) were taken directly from experimental results (Swansen, 1960) and were not optimized during the simulation. In addition, we constrained the bottom two layers of the slab to reflect the bulk Al$_2$O$_3$ geometry.
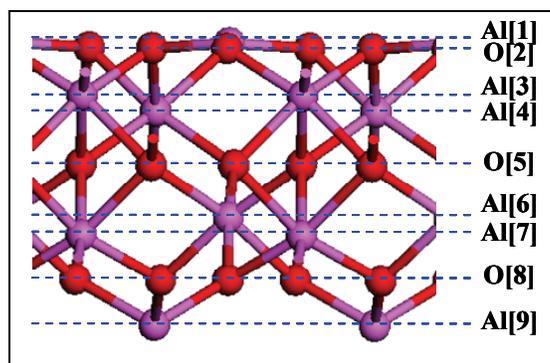
Figure 2.   Cross section of fully relaxed Al-terminated
αAl$_2$O$_3$ (0001) slab used for calculation.
The O and Al atoms are red and
magenta, respectively.

2.2   Model Parameters

All calculations were performed using ideal conditions (0 K, ultra high vacuum, defect free surface). The calculations were executed within the DMol^3 (Delley, 2000) module of the Materials Studio (version 4) software package using a double-numeric basis set with polarization functions (DNP) and the Perdew-Burke-Ernzerhof (PBE) (Perdue, 1996) version of the generalized gradient approximation (GGA) to represent the electron exchange and correlations. The ion cores were described by a density functional semi-core pseudopotential (DSPP) (Delley, 2002).

To validate our calculations, we compare our results for the surface reconstruction of the relaxed αAl$_2$O$_3$ (0001) slab with the results of other theoretical and experimental investigations (table 1). In agreement with other theoretical studies, our simulation predicts an 89% contraction of the

inter-atomic spacing of top surface layer and 6% expansion of the first sub-layer for the ultra-clean αAl_2O_3 (0001) surface. The predicted surface reconstruction was explained by Sousa et al. (1993) as being a result of charge redistribution due to the highly ionic nature of alumina. The experimental value for this relaxation is closer to ~50%. The discrepancy between theoretical prediction and experimental measurements may be due to the difficulty in preparing a perfectly terminated surface with no adsorbed atoms or defects.

Table 1. Comparison of theoretical and experimentally measured changes in the inter-atomic layer spacing of Al-terminated αAl_2O_3 (0001) slab with respect to their unrelaxed geometry.

	Theoretical							Experimental	
	Ours	**Hinneman**	**Verdozzi**	**Hass**	**Alavi**	**Ruberto**	**Carrasco**	**Guenard**	**Ahn**
#0xygen layers	3	9	18	3	3	9	11		
Functional	PBE/DSPP	PBE/PAW	LDA/NCPP	PBE/NCPP	PW91/USPP	PW91/NCPP	PBE/PAW		
$Al^{[1]}$-$O^{[2]}$	−89.2	−86.4	−87.4	−98	−97	−85.5	−93.8	−51	63
$O^{[2]}$-$Al^{[3]}$	+6	+4	+3.1	+5	+2	+3.2	+6.1	+16	
$Al^{[3]}$-$Al^{[4]}$	−39.9	−45.4	−41.7	−48	−53	−45.4	−46.7	−29	
$Al^{[4]}$-$O^{[5]}$	+18.9	+20.5	+18.3	+21	−27	+19.8	+22.0	+20	
$O^{[5]}$-$Al^{[6]}$	+17.1	+5	+5.6			+4.8	+8.5		
$Al^{[6]}$-$Al^{[7]}$	−31.2	−6.8	−8.3			−7.1	−11.6		
$Al^{[7]}$-$O^{[8]}$	0	+1.3	+1.1			+1.3	+2.2		
$O^{[8]}$-$Al^{[9]}$	0	−1.3	−0.5			−0.8	+0.7		
$Al^{[9]}$-$Al^{[10]}$		+4.6	+6.4			+3.0	+3.8		
$Al^{[10]}$-$O^{[11]}$		−1.2	−0.6			−0.7	−3.2		

To simulate adsorption phenomena, we added one adsorbate molecule per supercell, which is equivalent to approximately 1/12 monolayer according to Verdozzi et al. (1999), who define a monolayer as having one metal atom per surface oxygen. Binding energies were computed by subtracting the energy of the clean fully relaxed slab and the adsorbent molecule (H_2O, O_2, H_2) from the total energy of the system after adsorption. We performed barrier calculations using the linear synchronous transit (LST) method of Govind et al. (2003) to extrapolate between the reactant and product structures along the diffusion pathways illustrated in figure 3.
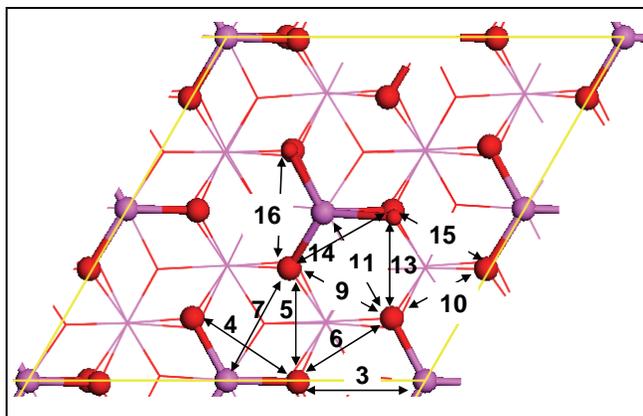
Figure 3. Top view of a 2x2 supercell showing allowed surface binding sites. The numbers correlate with the dissociation product and diffusion path notation referred to throughout the report. When referring to dissociation products, the endpoints of the line indicate the atoms to which the dissociated species bind.

2.3   Electron Spin State

The reaction chemistry of oxygen involved reactions on Al_2O_3 surfaces cannot be adequately described without careful consideration of the triplet-to-singlet spin conversion that occurs when the $2p\Pi_g$* orbitals hybridrize with the surface states. We find the energy difference between the triplet and the singlet ground state of free O_2 to be 19.3 kcal/mol, which is in good agreement with the experimentally measured value of 22.6 kcal/mol (Herzberg, 1950). Figure 4 shows adsorption structures and dissociation products for O, H, O_2, H_2, and H_2O on the Al-terminated αAl_2O_3 (0001) surface. For all adsorption/dissociation products except figure 4A, 4E, and 4J, the lowest energy spin state was singlet. In table 2, we detail the key molecular features for these structures as well as their binding energies. From table 2, it is clear that triplet states result in tighter O=O bonds and a local elongation of the $Al^{[1]}$-O bonding scheme. The spin state has no apparent effect on the length of hydroxyl or $Al^{[1]}$-$H^{[ads]}$ bonds. Based on the binding distances, it would appear that the triplet to singlet spin conversion occurs between 2 and 1.9Å above the surface for molecular O_2 and between 1.8 and 1.5 Å for atomic oxygen. However, this can only be verified by carefully sampling both the singlet and triplet potential energy surfaces as the adsorbing species approaches the surface.
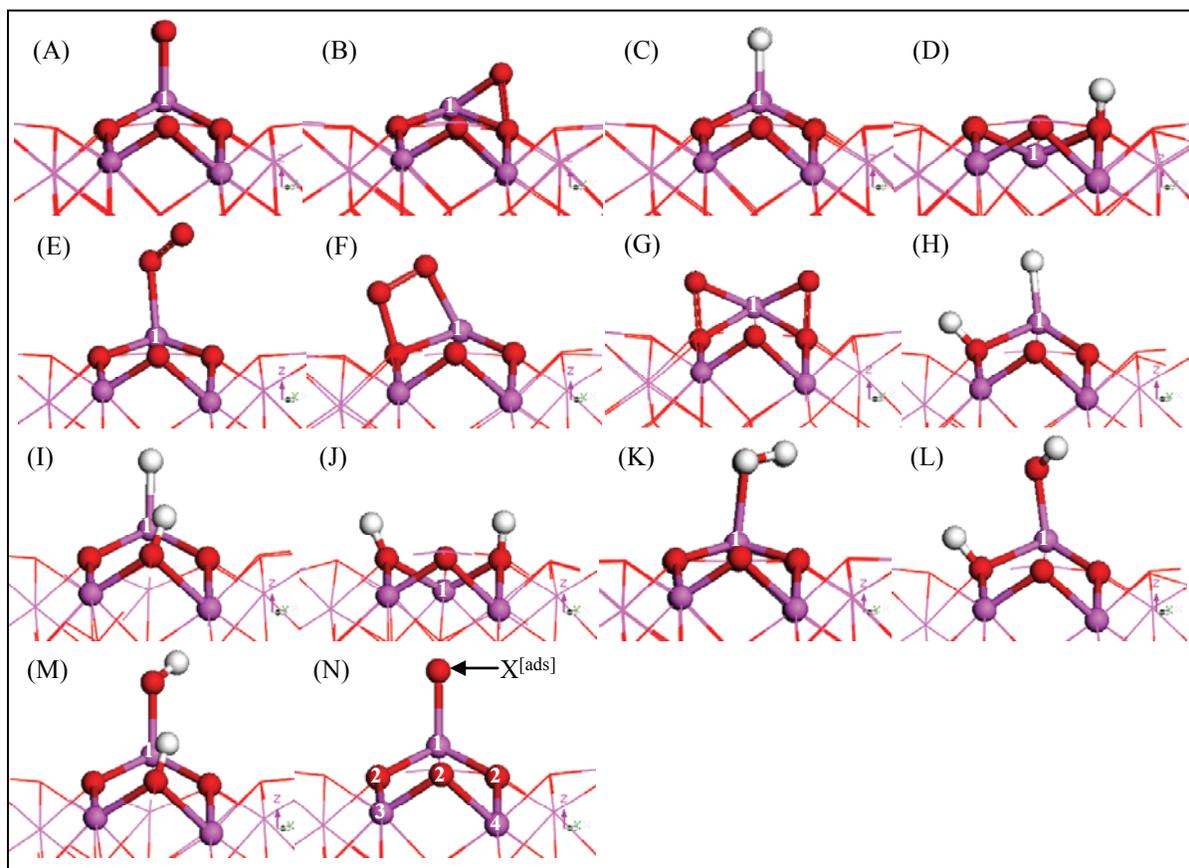
Figure 4. Adsorption and dissociated structures for (A) oxygen tetrahedron, (B) oxygen bridge, (C) hydrogen tetrahedron, (D) hydrogen, (E) 1-1 molecularly adsorbed O_2, (F) 1-2 dissociated O_2, (G) 2-2 dissociated O_2, (H) 1-2 dissociated H_2, (I) 1-4 dissociated H_2, (J) 2-2 dissociated H_2, (K) 1-1 molecularly adsorbed H_2O, (L) 1-2 dissociated H_2O, (M) 1-4 dissociated H_2O, and (N) the key indicating atomic layer to which atom originally belonged.

Table 2. Effect of spin state on O_2 adsorption binding energies and bond lengths. The ID notation refers to the structures in figure 4.

Atomic Oxygen Adsorption				
	$E_{binding}$	$O^{[ads]}$-$O^{[2]}$	$O^{[ads]}$-$Al^{[1]}$	$\angle$ bond
	(kcal/mol)	(Å)	(Å)	(°)
Triplet A	[-42][a]	-------	1.782	112
Singlet A	-30 [-35] [a]	-------	1.767	115
Triplet B	[-18][a]	1.508	1.797	49
Singlet B	-49 [-53] [a]	1.546	1.803	50
Atomic Hydrogen Adsorption				
	$E_{binding}$	$H^{[ads]}$-$O^{[2]}$	$H^{[ads]}$-$Al^{[1]}$	$\angle$ bond
Triplet C	-20	----------	1.626	114
Singlet C	-36	----------	1.625	114
Triplet D	-98	0.971	-------	124
Singlet D	-116	0.972	-------	124
Molecular Oxygen Adsorption / Dissociation				
	$E_{binding}$	O=O	$O^{[ads]}$-$Al^{[1]}$	$\angle$ bond
Triplet E	-7	1.255	1.997	107
Singlet E	-13	1.276	1.959	110
Triplet F	21	1.364	1.895	74
Singlet F	-3	1.393	1.851	76
Triplet G	51	1.499	1.837	48
Singlet G	25	1.522	1.823	49
Molecular Hydrogen Dissociation				
	$E_{binding}$	$H^{[ads]}$-$O^{[2]}$	$H^{[ads]}$-$Al^{[1]}$	$\angle$ bond
				OH,HOAl
Triplet H	-15	0.982	1.594	110, 120
Singlet H	-14	0.981	1.593	110, 120
Triplet I	-14	0.971	1.621	120, 113
Singlet I	-10	0.972	1.615	121, 112
Triplet J	-85	0.973	------	127, ----
Singlet J	-67	0.973	------	127, ----
H_2O Adsorption / Dissociation				
	$E_{binding}$	$H^{[ads]}$-$O^{[2]}$	$O^{[ads]}$-$Al^{[1]}$	$\angle$ OAlO
				OH,OAlO
Triplet K	-27 [-23] [b]	0.982	1.982	----, 87
Singlet K	-26 [-23] [b]	0.983	1.987	----, 86
Triplet L	-40 [-33] [b]	0.982	1.740	110, 112
Singlet L	-38 [-33] [b]	0.981	1.740	109, 114
Triplet M	-38 [-33] [b]	0.972	1.759	121, 97
Singlet M	-34 [-33] [b]	0.973	1.758	122, 97

[a]The number in brackets is from Gamallo, 2007
[b]The number in brackets is from Haas, 2000.

Since an objective of this research is to establish whether dissociated oxygen from the alumina support can diffuse to the catalytic particle and all possible surface diffusion pathways include a bridging conformation, we chose to perform our barrier calculations using a singlet spin state for both the reactant and products. This is the most accurate method to explore the effects of crystal symmetry and surface reconstructions on the dissociation and diffusion barriers for reaction

pathways that do not involve a spin change. In future studies, we will perform a detailed sampling of both the triplet and singlet potential energy surfaces using the constrained geometry method to assess the reaction barriers for pathways that involve spin-to-triplet transformations

3. Results and Discussion

3.1 Effects of Adsorption on Surface Reconstruction

In table 3, we demonstrate the effect of the adsorption of different species on both the local and long-range reconstruction of the αAl_2O_3 (0001) surface. Both H and O can directly bind with similar binding energies ($\sim$ -30 kcal/mol) to the surface $Al^{[1]}$ forming a tetrahedron with neighboring $O^{[2]}$ atoms. By saturating the surface $Al^{[1]}$, the O^{ads} reduces the driving force for the contraction of the first inter-atomic layer. Although H binds closer to the surface $Al^{[1]}$ than O, both H and O produce the same elongation of the local $Al^{[1]}$-$O^{[2]}$ bonding scheme. H and O can also directly bind to the $O^{[2]}$ atoms.   However, in this configuration, there are significant differences in both the adsorption structures and binding energies ($E_{bind}^{O} \sim$ -50, $E_{bind}^{H} \sim$ -116kcal/mol). Whereas O pulls the $Al^{[1]} \sim$ 8% away from the surface, H drives $Al^{[1]}$ deeper into the lattice. The closer the binding site is to an $Al^{[1]}$ site, the deeper it is driven into the lattice and the greater the asymmetrical lengthening of the local $Al^{[1]}$-$O^{[2]}$ bonding scheme. This has a profound effect on the relaxation of the top two inter-atomic layers. As the surface $Al^{[1]}$ is driven into the lattice, it reduces the ability of the oxygen layer to charge compensate for excess charge on the remaining unsaturated surface aluminum atoms, resulting in a smaller contraction of the first inter-atomic layer.

Table 3. Effect of adsorption on surface reconstruction.

	Layer1 (%)	Layer2 (%)	$\Delta Al^{[1]}$ (%)	$Al^{[1]}-O^{[2]}$ Å		
Al_2O_3	-89	+6	–	1.704	1.704	1.704
O (A)	-83	+6	+11	1.783	1.783	1.783
O (B)	-98	+9	+8	1.826	1.715	1.714
H (C)	-87	+6	+11	1.784	1.784	1.784
H (D)	Non uniform		-14	1.841	1.747	1.746
O_2 (E)	-90	+7	+7	1.735	1.735	1.733
O_2 (F)	-84	+4	+9	1.878	1.711	1.710
O_2 (G)	-86	+13	+13	1.869	1.862	1.733
H_2 (H)	-83	+10	+13	1.920	1.764	1.764
H_2 (I)	-84	+9	+11	1.796	1.790	1.770
H_2 (J)	Non uniform		-16	1.844	1.837	1.745
H_2O (K)	-104	+6	+6	1.733	1.721	1.720
H_2O (L)	-83	+9	+13	1.894	1.755	1.755
H_2O (M)	-85	+7	+11	1.793	1.779	1.766

Note: Layer 1 and Layer 2 are the percent change in the 1st and 2nd inter-atomic layers with respect to their bulk coordinates. A negative sign for Layer 1or 2 represents a contraction of the layer. $\Delta X^{[bind]}$ calculates how much the adsorbate pulls the surface $Al^{[1]}$ site from its original relaxed position. $Al^{[1]}-O^{[2]}$ are the surface bonds neighboring the adsorption site.

O_2 and H_2O can molecularly adsorb to surface $Al^{[1]}$ with binding energies of ~20kcal/mol; whereas, H_2 cannot. O_2 adsorbs closer to the surface than H_2O and does not change the contraction of the first inter-atomic layer. In contrast, molecularly adsorbed H_2O causes the surface $Al^{[1]}$ to contract below the $O^{[2]}$ atoms, changing the surface termination from Al-terminated to O-terminated although the Al and O atoms are nearly co-planar.

As shown in figure 4, there are three unique configurations for the dissociated products, henceforth referred to as 1-2, 1-4, and 2-2 dissociation. H_2 can form all three dissociation products; however, H_2O cannot form 2-2 dissociation products and O_2 cannot form 1-4 dissociation products. In comparing the dissociation products, the following trends are clear: (1) dissociation reduces the contraction of the first inter-atomic layer regardless of which species is dissociating and (2) $E_{bind} O_2 > E_{bind} H_2 > E_{bind} H_2O$. In regards to which type of dissociation product has the lowest energy, it depends on which species are present. For both H_2O and O_2, the lowest energy dissociation products are 1-2; however, for H_2, the lowest energy dissociation product is 2-2.

3.1 O_2 Molecular and Dissociative Adsorption

The molecular and 1-2 dissociative adsorption of O_2 from free O_2 appears to be spontaneous. However, the actual barrier for direct and indirect (i.e., from 1-2 molecularly adsorbed) dissociation cannot be determined using the LST transition state method because the reaction involves a triplet-singlet spin conversion, which can only be accurately described by sampling both the triplet and singlet potential energy surfaces. Nevertheless, we can accurately calculate

the barriers to the further dissociation of 1-2 into 2-2 products since the minimum energy structure for both of these structures is a singlet spin state. We find that the further dissociation of 1-2 adsorption products is highly endothermic and not kinetically favorable ($E_{rxn} = 28$ kcal/mol, $E_{barrier} = 53$ kcal/mol). Given these results, the indirect dissociation of O_2 is not considered a viable source for isolated substrate bound atomic oxygen.

3.2 H_2O Adsorption and Dissociation

The question arises as to whether dissociated H_2O can serve as a source of substrate bound oxygen. To answer this question, we investigated the following five pathways for the adsorption and dissociation of H_2O:

1. Free H_2O molecularly (figure 4K) adsorbs to Al[1].

2. Free H_2O dissociates into a 1-2 conformation (figure 4L) by forming hydroxyls with Al[1] and its first nearest neighboring O[2].

3. Free H_2O dissociates into a 1-4 conformation (figure 4M) by forming hydroxyls with Al[1] and its second nearest neighboring O[2].

4. Adsorbed H_2O (figure 4K) dissociates into a 1-2 conformation.

5. Adsorbed H_2O (figure 4K) dissociates into a 1-4 conformation.

Our results indicate that H_2O spontaneously dissociates into both 1-2 and 1-4 conformations. Both dissociated products have equivalent adsorption energies. H_2O can also adsorb molecularly to surface Al with a slightly higher energy than its dissociated product (~+10kcal/mol). The barrier for the molecular adsorption of H_2O is 0.083 kcal/mol, which is within the limits of the accuracy of the model. Once molecularly adsorbed, the barrier to further dissociation into 1-2 and 1-4 products are 23 and 9.6 kcal/mol, respectively. Experimentally (Elam, 1998), there has been no evidence found for the existence of molecularly adsorbed H_2O. Since the energy released due to spontaneous dissociation from free H_2O is well in excess of the barriers for dissociation from molecular H_2O, our results suggest that if molecular H_2O exists on the surface, it is unlikely to have a long lifetime.

The next series of questions that arise is (1) Can hydrogen diffuse away from dissociated H_2O? and (2) Can the remaining Al[1]OH hydroxyl group further dissociate into a H and O pair? We find that the easiest paths for the H to diffuse away from dissociated H_2O are paths 10, 13, 15 ($E_{barrier} \sim$ 17–24 kcal/mol). These paths avoid the influence of Al[1] and Al[3] atoms. For all other paths considered, the barrier to the diffusion of H from dissociated H_2O was >40 kcal/mol. The barrier to the further dissociation of the remaining Al[1]OH hydroxyl into 2-2 and 2-4 O••H dissociation pairs is 45 and 34 kcal/mol, respectively.

3.3 O Surface Diffusion

The final question to be answered is whether the isolated substrate bound O that is produced from the dissociation of H_2O can diffuse across the Al_2O_3 surface to the catalytic particle to promote combustion. In table 4, we provide barrier calculations for diffusion of O and H between all allowed surface sites. We find that O can easily diffuse from $Al^{[1]}$ tetrahedron (figure 4A) to a bridging (figure 4B) conformation ($E_{barrier} = 4$ kcal/mol). Once in a bridging conformation, O can diffuse between bridging sites that neighbor the same surface $Al^{[1]}$ ($E_{barrier} = 27$ kcal/mol). However, jumping to bridging sites on a different surface $Al^{[1]}$ atom requires a minimum of 47 kcal/mol. We also calculated the diffusion barrier for a concerted diffusion path in which $O^{[ads]}$ displaces an $O^{[2]}$, which then moves into a bridging site on the neighboring $Al^{[1]}$. The barrier to concerted O diffusion is 61 kcal/mol. These results suggest that in the absence of any other species, O becomes localized near the surface $Al^{[1]}$ sites. However, several of the diffusion paths involve singlet to triplet conversion and need to be further studied before this conclusion can be confirmed.

Table 4. Surface diffusion of bound O and H.

Path ID	Oxygen $E_{barrier}$	Hydrogen $E_{barrier}$	H assisted O $E_{barrier}$
1	4	18	–
2	4	18	–
12	22	99	–
4	27	42	1
14	27	42	3
16	47	42	3
5	46	34	45
6	47	34	46
9	67	34	43
10	65	18	48
13	64	19	48
15	64	19	46
3	68	34	–
7	49	25	–
11	68	107	–

Note: O diffusion along paths 1, 2, 12, 3, 7, and 11 involves a
triplet-singlet spin change and must be studied in more
detail before the diffusion barriers can be verified.

We also studied whether the presence of pre-adsorbed H can promote O diffusion. We find that pre-adsorbed H nearly eliminated the barriers to O diffusion around $Al^{[1]}$ sites and reduced the barriers along paths 10, 13, and 15 by 17 kcal/mol. However, this improvement was not adequate to allow O to completely transverse a unit cell. Alternatively, when O and H are allowed to diffuse as a pair, the maximum barrier encountered while traversing the unit cell is 24 kcal/mol. These results suggest that the presence of both mobile O and H species are required for O surface diffusion.

3.4 H₂ Dissociation

H_2 cannot molecularly adsorb to the Al terminated αAl_2O_3 surface; however, it is both thermodynamically and kinetically favorable for H_2 to dissociate into 1-4 ($E_{barrier}$ = 20 kcal/mol, E_{rxn} = -9 kcal/mol) and 2-2 ($E_{barrier}$ = 2 kcal/mol, E_{rxn} = -60 kcal/mol) dissociation products. These results support the experimental measurements of Wang (1996), who postulated that H_2 adsorbed to the Al_2O_3 support resulted in a dramatic increase in the H_2 response during temporal analysis of products (TAP).

3.5 H Surface Diffusion

From the results in table 4, we find that H can diffuse from a $Al^{[1]}$ tetrahedron site (figure 4C) to either the first ($E_{barrier}$ = 18 kcal/mol) or second nearest neighboring O atom ($E_{barrier}$ = 26 kcal/mol). Once in these conformations, diffusion between $O^{[2]}$ sites neighboring the same surface $Al^{[1]}$ site is unlikely ($E_{barrier}$ = 42 kcal/mol). However, H can diffuse between $O^{[2]}$ sites neighboring different $Al^{[1]}$ sites with barriers of 18 and 34 kcal/mol, depending on how close the sub-surface Al atoms are to the diffusion path.

4. Conclusions

In summary, we provide a theoretical model for reaction processes that occur on the Al_2O_3 substrate and influence combustion at the catalytic particle. Our model suggests that H_2O is a primary source of mobile O and H species. Once dissociated, H can diffuse away from dissociated H_2O leaving behind an $Al^{[1]}$–OH hydroxyl, which can also further dissociate creating a 2-2 O••H pair. Although isolated O atoms encounter large barriers to surface diffusion, the 2-2 dissociated O••H pair can diffuse with a barrier ~24 kcal/mol. We also find that H_2 dissociation is an active source of mobile H species. Although O_2 can adsorb molecularly, it cannot further dissociate to create mobile O. However, given that the presence of pre-adsorbed H had a profound influence on the surface diffusion of O, it may be likely that H can also influence the dissociation of molecularly adsorbed O_2.

5. References

Ahn, J.; Rabalais, J. W. Composition and Structure of the αAl$_2$O$_3$ {0001}-(1x1) Surface. *Surf. Sci.* **1997**, *388*, 121–131.

Alavi, S.; Sorescu, D. C.; Thompson, D. L. Adsorption of HCl on Single-Crystal αAl$_2$O$_3$ Surfaces: a DFT Study. *J. Phys. Chem. B* **2003**, *107*, 186–195.

Carrasco, J.; Gomes, J.; Illas, F. Theoretical Study of Bulk and Surface Oxygen and Al Vacancies in αAl$_2$O$_3$. *Phys. Rev. B* **2004**, *69*, 064116(1–13).

Delley, B. From Molecules to Solids with the Dmol3 Approach. *J. Chem. Phys.* **2000**, *113*, 7756–7764.

Delley, B. Hardness Conserving Semi-Local Pseudopotentials. *Phys. Rev. B* **2002**, *66*, 155125(1–9).

Elam, J. W.; Nelson, C. E.; Cameron, M. A.; Tolbert, M. A.; George, S. M. Adsorption of H$_2$O on a Single Crystal αAl$_2$O$_3$ (0001) Surface. *J. Phys. Chem. B* **1998**, *102*, 7008–7015.

Guenard, P.; Renaud, G.; Barbier, A.; Gautier-Soyer, M. Determination of αAl$_2$O$_3$ (0001) Surface Relaxation and Termination by Measurements of Crystal Truncation Rods. *Surf. Rev. Lett.* **1998**, *5*, 321–324.

Govind, N.; Peterson, M.; Fitzgerald, G.; King-Smith, D.; Andzelm, J. A Generalized Synchronous Transit Method for Transition State Location. *Comp. Mat. Sci.* **2003**, *28*, 250–258.

Hass, K. C.; Schneider, W. F.; Curioni, A.; Andreoni, W. First Principles Molecular Dynamics Simulations of H$_2$O on αAl$_2$O$_3$ (0001). *J. Phys. Chem. B* **2000**, *104*, 5527–5540.

Herzberg, G. *Molecular Spectra and Molecular Structure, I. Spectra of Diatomic Molecules*; Van Nostrand Reinhold Company, New York, 1950.

Hinnemann, B.; Carter, E. Adsorption of Al, O, Hf, Y, Pt and S Atoms on αAl$_2$O$_3$ (0001). *J. Phys. Chem. C* **2007**, *111*, 7105–7126.

Marmier, A.; Parker, S. Ab Initio Morphology and Surface Thermodynamics of αAl$_2$O$_3$. *Phys. Rev. B* **2004**, *69*, 115409(1–9).

Mhadeshware, A. B.; Vlachos, D. G. A Catalytic Reaction Mechanism for Methane Partial Oxidation at Short Contact Times, Reforming and Combustion, and of Oxygenate Decomposition and Oxidation on Pt. *Ind. Eng. Chem. Res.* **2007**, *46*, 5310–5324.

Norton, D. G.; Voit, K. W.; Bruggemann, T.; Vlachos, D. G. Portable Power Generation via Integrated Catalytic Microcombustion-Thermoelectric Devices. *Proc. 24th Army Science Conference*, 2004.

Perdew, J. P.; Burke, K.; Ernzerhof, M. Generalized Gradient Approximation Made Simple. *Phys. Rev. Lett.* **1996**, *77*, 3865–3866.

Ruberto, C.; Yourdshahyan, T.; Lundqvist, B. Surface Properties of Meta-stable Al_2O_3: A Comparative Study of κ and $αAl_2O_3$. *Phys. Rev. B* **2003**, *67*, 195412(1–18).

Sousa, C.; Illas, F.; Pacchioni, G. Can Corundum be Described as an Ionic Oxide? *J. Chem. Phys.* **1993**, *99*, 6818–6823.

Swanson, H. E.; Cook, M. I.; Evans, E. H.; de Groot, J. H. Standard X-Ray Diffraction Powder Patter NBS Circular no 539, 10, 3, U.S. Government Printing Office: Washington, DC, 1960.

Verdozzi, C.; Jennison, D.; Schultz, P.; Sears, M. Sapphire (0001) Surface, Clean and with d-Metal Overlayers. *Phys. Rev. Lett.* **1999**, *82*, 799–802.

Wang, D.; Dewaele, O.; Groote, G. F. Reaction Mechanism and Role of the Support in the Partial Oxidation of Methane on Rh/Al_2O_3. *J. Catalysis* **1996**, *159*, 418–426.